

# Exploring Nonlinear Flame Speed Inhibition Effects in Mixtures of R1234yf and R32 under Microgravity Conditions\*

Raik Hesse<sup>a,\*</sup>, Roman Glaznev<sup>a</sup>, Raymond Langer<sup>a</sup>, Christian Schwenzer<sup>a</sup>, Valeri Babushok<sup>b</sup>, Gregory Linteris<sup>b</sup>, Heinz Pitsch<sup>a</sup>, Joachim Beeckmann<sup>a</sup>

<sup>a</sup>*Institute for Combustion Technology, RWTH Aachen University, Templergraben 64, 52056 Aachen, Germany*

<sup>b</sup>*National Institute of Standards and Technology, Gaithersburg, MD, USA*

---

## Abstract

This study investigates the flame speed inhibition effects in R1234yf and R32 mixtures, two hydrofluorocarbon (HFC) refrigerants with low global warming potential but mild flammability. The laminar flame speed ( $S_{L,u}^0$ ) is a crucial parameter for assessing fire potential, and this research aims to provide high-fidelity flame speed data for refining chemical kinetic models. The slow flame propagation behavior of these refrigerants poses a formidable challenge to measurements due to buoyancy and radiation effects. This study simultaneously obtains  $S_{L,u}^0$  data using optical (Schlieren) and pressure-rise methods under microgravity conditions, allowing for comprehensive and accurate data acquisition. Initial conditions of 3 bar and 333 K were used to mitigate contamination by stretch effects. Additionally, data for R1234yf were provided for extrapolation to standard conditions, enabling comparisons with literature data. Our results reveal substantial nonlinear blending effects on the laminar flame speed by introducing small fractions of R1234yf into R32 mixtures. While the selected kinetic model showed promising predictions, it could not fully predict the observed strong nonlinear flame speed decrease in experiments due to R1234yf addition. Chemical kinetic model analyses, including flux and sensitivity analyses, were employed to understand the blending interactions. The study highlights that the addition of R1234yf leads to the formation of HF, trapping radicals and inhibiting chain-branching reactions. Sensitivity analysis indicates that reactions involving fuel-specific intermediates ( $\text{CHF}_2$  for R32 and  $\text{CF}_3$  for R1234yf) play a key role. Specifically,  $\text{CHF}_2$  supplies H-atoms, while  $\text{CF}_3$  drains H-atoms. Hence, the introduction of R1234yf leads to a reduction in flame temperature, the creation of an extended post-flame zone, and a substantial decrease in  $S_{L,u}^0$ .

*Keywords:* Laminar flame speed; Refrigerant flammability; R32; R1234yf; Microgravity;

---

\*Official contribution of NIST, not subject to copyright in the United States. Certain commercial equipment, instruments, and materials are identified in this paper to adequately specify the procedure. Such identification does not imply recommendation or endorsement by the National Institute of Standards and Technology.

## 1. Introduction

Refrigerants with a high global warming potential (GWP) are being replaced with low-GWP substitutes. The reduced atmospheric lifetimes, however, often come with mild flammability. Therefore, it is essential to understand their level of flammability. For safety evaluation, the laminar flame speed  $S_{L,u}^0$  is an important property characterizing the combustion process. Compared to hydrocarbons, the amount of experimental and modeling studies on these hydrofluorocarbon (HFC) refrigerants is sparse, making accurate experimental data extremely valuable for constraining uncertainties of chemical kinetic models. However, obtaining accurate data is also extremely challenging because of their often very low flame speeds.

Difluoromethane ( $\text{CH}_2\text{F}_2$ , R32) and 2,3,3,3-tetrafluoro-1-propene ( $\text{CH}_2=\text{CFCF}$ , R1234yf, short: "yf") are two low-GWP HFCs with estimated 100-year GWPs of 809 and 1 (Hodnebrog et al. [1]), respectively. By mixing refrigerants, flammability, refrigerant cycle performance, stability, and low GWP properties can be tuned to obtain high-potential drop-in solutions for existing systems [2]. However, delineating the flammability characteristics of marginally flammable refrigerants and their blends is difficult. For example, R32 and R1234yf were reported by Takizawa et al. [3, 4] with peak laminar flame speeds at standard conditions<sup>1</sup> of 6.7 cm/s and 1.2 cm/s, respectively. Accurate assessment of the combustion characteristics of these refrigerants places particular demands on laminar flame speed measurement methods.

Due to the larger time scales of slowly propagating refrigerant flames, two physical phenomena dominate: (1) The buoyancy-induced deformation of the flames and (2) the radiation heat losses. These alter the flames not only on a kinematic but also on a chemical level and complicate flame speed estimates employing conventional methods. The flame speed of a refrigerant is analyzed in vertical cylindrical tubes (VT) made of glass, e.g., [5, 6] or in closed combustion vessels (CV), e.g., [3, 4, 7, 8]. The latter method determines  $S_{L,u}^0$  by measuring the radius evolution of an outwardly propagating flame (OPF) using optical methods (O) such as Schlieren diagnostics or the pressure-rise trace (P) during the near isentropic compression phase. Available flame speed studies on R32 and R1234yf are summarized in the Supplementary Materials in Tab. S1. Only a minority of studies consider radiation effects with an optically thin gas model (OTM) and conduct experiments under microgravity ( $\mu g$ ) to suppress buoyancy. Thus, chemical kinetic model development for HFC combustion prediction, e.g., by Papas et al. [6], Needham and Westmoreland [9], and Babushok et al. [10], partly relies on flame speed data, where radiation, buoyancy, and often stretch effects remain unconsidered. The present work addresses these challenges to provide accurate

data.

In a previous study [8], we compared the optical and pressure-rise methods to address ambiguities in calculating the laminar flame speed for slowly propagating R32 flames under terrestrial condition ( $g$ ) and microgravity ( $\mu g$ ). By thoroughly identifying data deduction limits for optical and pressure-rise methods, flames with  $S_{L,u}^0$  below 5 cm/s can be investigated, provided that effects of radiation heat losses are estimated and corrected. To effectively reduce stretch effects, experiments can be conducted at elevated pressures. These measures enable the acquisition of accurate data for kinetic model validation.

For this study, high-fidelity measurements were conducted to investigate the blending behavior of mixtures containing R32/R1234yf/air. To eliminate uncertainties arising from buoyancy, mixtures with R1234yf were measured under  $\mu g$ . The collected data provides a solid basis to answer the following research questions: (1) How does the addition of R1234yf affect the flame speed of R32? (2) How can we describe the blending behavior? (3) What are the chemical processes occurring in these blends?

## 2. Experimental framework

Microgravity experiments were conducted in ZARM's (Center of Applied Space Technology and Microgravity) high-repetition drop tower facility called the GraviTower Bremen Pro (GTB Pro) providing up to 2.5 s weightlessness of less than  $10^{-4} g$  during drops. For details of the experimental setup, we refer to our previous descriptions [8]. A brief introduction is also included in the Supplementary Materials.

This study conducted experiments with various R32/R1234yf blending ratios of  $X_{yf} \in [0, 0.15, 0.3, 0.5, 1]$  and equivalence ratios of  $\phi = 1.1$  and 1.3, which are expected to encompass peak flame speed positions, at a pressure of  $p_0 = 3$  bar and a temperature of  $T_0 = 333$  K. Fuel-air equivalence ratio sweeps were conducted for pure R32 and R1234yf at the same initial pressure and temperature. In order to relate our findings at high pressures to standard conditions, we performed flame measurements of R1234yf/air for  $\phi = 1.3$  along the isentropic compression line that corresponds to standard conditions. The collected flame speed data along this isentrope was used to determine the flame speed at standard conditions by extrapolation.

## 3. Flame speed determination

### 3.1. Optical method

Flame front extraction is limited to spherically smooth flame fronts above a critical radius associated with the complete decay of ignition artifacts and within a quasi-isobaric regime. The temporal evolution of the flame front radius ( $R_f$ ) is measured at its

<sup>1</sup>Standard conditions refer to 1.01325 bar and 298 K.

1 iso-temperature surface of approximately 850 K using  
 2 Schlieren images. Central differences are applied  
 3 to obtain the stretched propagation speed of a burned  
 4 mixture  $S_{L,b} = \dot{R}_f = dR_f/dt$ , assuming quiescent  
 5 burned gases. An OPF's stretch rate  $K$  is defined as  
 6 the temporal change of the flame surface area  $A$  leading  
 7 to  $K = 1/A_f \cdot dA_f/dt = 2/R_f \cdot dR_f/dt$ . The  
 8 nonlinear expression provided by Kelley et al. [11]  
 9 is used to calculate the unstretched flame speed  $S_{L,b}^0$   
 10 denoted with the superscript "0" and the Markstein  
 11 length  $\mathcal{L}_b$ . The unstretched laminar flame speed of  
 12 the unburned gas,  $S_{L,u}^0$ , can be evaluated for adia-  
 13 batic flames by mass continuity through a planar un-  
 14 stretched flame,  $S_{L,u}^0 = S_{L,b}^0 (\rho_b/\rho_u)$ , where  $\rho_b$  and  
 15  $\rho_u$  are the burned and unburned densities. A slowly  
 16 burning flame can render this relation invalid due  
 17 to radiation heat loss, inducing a contraction veloc-  
 18 ity (kinematic effect) and a temperature decrease in  
 19 the reaction zone (chemical effect), as discussed by  
 20 Hesse et al. [12]. Recently, Tavares et al. [13] im-  
 21 proved the correction of the kinematic effect, empha-  
 22 sizing an important coupling of convective terms in  
 23 the energy and continuity equations. The model pre-  
 24 dicts contraction velocities for R32 but deviates for  
 25 R1234yf flames due to the slow oxidation of CO to  
 26 CO<sub>2</sub>, common in HFC flames with F/H > 1. Inter-  
 27 preting the larger fractions of CO in the burned gas  
 28 as CO<sub>2</sub> leads to overestimating the radiation heat loss  
 29 due to the CO<sub>2</sub>'s larger Planck-mean absorption coef-  
 30 ficients. Their results imply that corrections of flame  
 31 measurements under elevated pressures, which is the  
 32 subject of the present study, are less affected because  
 33 of their thinner reaction zone. Hence, corrections ac-  
 34 cording to Tavares et al. are applied to optical method  
 35 results, and radiation effects on the chemistry are es-  
 36 timated using Santner et al.'s [14] model based on  
 37 the activation temperature, as previously applied for  
 38 R32 flames in Hesse et al. [8, 12].

### 39 3.2. Pressure-rise method

40 Several assumptions are invoked to calculate  $S_{L,u}$   
 41 from pressure-rise data, including infinitely thin  
 42 smooth spherical flame fronts during combustion,  
 43 spatially uniform pressure during combustion, isen-  
 44 tropic compression of unburned gases, ideal gases,  
 45 equilibrium of burned gases, and negligible radia-  
 46 tion and buoyancy effects. In Bariki et al. [15],  
 47 we recently discussed this method and its errors in  
 48 fast-burning flames using a two-zone model. For  
 49 slowly burning flames, as investigated in the present  
 50 study, a multi-zone model, such as the Mass- and  
 51 Energy-Conserving Thermo (MECT) introduced by  
 52 Elia et al. [16], is required to incorporate radiation  
 53 heat losses. Here, we selected the National Institute  
 54 of Standards and Technology's (NIST) data reduc-  
 55 tion tool for spherical constant volume flame experi-  
 56 ments [17], which uses the MECT multi-zone model.  
 57 Pressure data were processed by applying a moving  
 58 average scheme. Radiation effects were modeled in  
 59 the burned equilibrated gas for the species CO<sub>2</sub>, CO,

60 H<sub>2</sub>O, CF<sub>2</sub>O, and HF, using the optically thin model  
 61 (OTM), thus assuming the absence of radiation ab-  
 62 sorption. Handling radiation in a statistical narrow-  
 63 band model framework is impossible due to the lack  
 64 of radiation absorption parameters of some important  
 65 species at appropriate combustion temperatures.

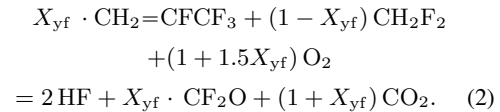
66 A power law functional relationship is commonly  
 67 used for extrapolating flame speeds to initial temper-  
 68 atures  $T_0$  and pressures  $p_0$ , expressed as

$$S_{L,u} = S_{L,u,0} \left( \frac{p}{p_0} \right)^\alpha, \text{ and } T = T_0 \left( \frac{p}{p_0} \right)^{\frac{\gamma-1}{\gamma}}, \quad (1)$$

69 where  $S_{L,u,0}$  is the laminar flame speed at  $p_0$  and  $T_0$ ,  
 70 and the exponent  $\alpha$  depends on the mixture compo-  
 71 sition. The corresponding temperature  $T$  along the  
 72 near-isentropic compression is given by the second  
 73 equation, with  $\gamma$  being the isentropic exponent with  
 74 respect to the unburned gas.

## 75 4. Results and discussion

76 The reaction stoichiometry used to describe  
 77 HFC/air mixtures in this study was defined by Tak-  
 78 izawa et al. [18] for refrigerants containing equal or  
 79 less fluorine than hydrogen atoms, e.g., R32 (CH<sub>2</sub>F<sub>2</sub>),  
 80 and those containing more fluorine than hydrogen  
 81 atoms, e.g., R1234yf (CH<sub>2</sub>=CFCF<sub>3</sub>), which are com-  
 82 bined via the molar fraction  $X_{yf}$  of R1234yf in the  
 83 refrigerant mixture:



### 84 4.1. Optical method results

85 Figure 1 depicts the flame evolutions of  
 86 R32 and R1234yf/air mixtures at an equiva-  
 87 lence ratio of 1.1 obtained with the optical method.  
 88 R32/air flames propagate about three times faster  
 89 than R1234yf/air flames, as indicated by the local  
 90 propagation speeds  $\dot{R}_f$  above the flame images.

91 Flames expand spherically without apparent arti-  
 92 facts caused by the electrodes. Although the present  
 93 study was conducted at high ignition pressures of  
 94  $p_0 = 3$  bar, flame wrinkling due to hydrodynamic  
 95 or thermodiffusive instability is not an issue. Particu-  
 96 larly, it is not observed for richer flames of  $\phi = 1.5$   
 97 and elevated pressures along the near-isentropic com-  
 98 pression, relevant for pressure-rise data evaluation.  
 99 Figure 2 presents the relationship between the propa-  
 100 gation speed  $\dot{R}_f$  and the flame's stretch rate  $K$  for  
 101 both neat refrigerants and a blend of  $X_{yf} = 0.15$  with  
 102  $\phi = 1.1$ ,  $p_0 = 3$  bar, and  $T_0 = 333$  K. The data was cor-  
 103 rected for radiation-induced contraction velocities us-  
 104 ing the code from Tavares et al. [13]. The flame propa-  
 105 gation can be subdivided into three regimes associ-  
 106 ated with (I) ignition energy decay, (II) transition to

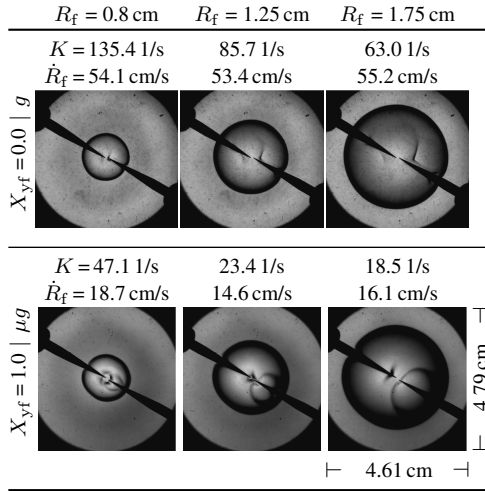


Fig. 1: Flame recordings at  $\phi = 1.1$ ,  $X_{O_2, \text{air}} = 20.94 \%$ , 333 K, and 3 bar at the volume equivalent radius  $R_f$ .

1 self-sustained propagation, (III) self-sustained flame  
 2 propagation. Only (III) was selected for extrapolation  
 3 to zero stretch rates.

4 Adding a fraction of  $X_{yf} = 0.15$  to R32 drastically  
 5 decreases the propagation speeds by 30 % and in-  
 6 creases the Markstein length  $\mathcal{L}_b$  from 0.66 mm to  
 7 0.95 mm.  $\mathcal{L}_b$  further increases for neat R1234yf/air  
 8 to 2.4 mm. These findings lead to a pronounced  
 9 nonlinear blending behavior of  $S_{L,u}^0$  for R1234yf-  
 10 addition. The already large Markstein lengths for neat  
 11 R1234yf/air flames at 3 bar and 333 K should be even  
 12 larger for standard conditions, because  $\mathcal{L}_b$  is propo-  
 13 rotional to the flame thickness, which increases toward  
 14 lower pressures. Thus, the small optically accessi-  
 15 ble radius of about 2 cm in the present work makes  
 16 extrapolations to zero stretch more uncertain, which  
 17 is the reason why elevated pressures are beneficial  
 18 in small combustion vessels, as discussed by Beeck-  
 19 mann et al. [19]. This also applies to the pressure-rise  
 20 method, where stretch, ignition residues, and electri-  
 21 cal noise can influence the lower data range.

#### 22 4.2. Pressure-rise method results

23 The measured flame speeds from the pressure-rise  
 24 method for the neat R1234yf/air mixtures at  $\phi = 1.1$   
 25 are presented in Fig. 3. These flame speeds are al-  
 26 ready converted to the unburned conditions, so they  
 27 are referred to as the laminar flame speed  $S_{L,u}$ . Note  
 28 that  $S_{L,u}$  is not strictly referring to the unstretched  
 29 laminar flame speed  $S_{L,u}^0$ , as it might still be slightly  
 30 stretch-affected at small flame radii and correspond-  
 31 ing low pressures. To prevent  $S_{L,u}$  values from be-  
 32 ing contaminated by stretch effects, data must be se-  
 33 lected and extrapolated to the initial conditions at  $p_0$   
 34 and  $T_{u,0}$ . A lower limit of  $p \gtrsim 1.4p_0$  to  $2p_0$  was found  
 35 to satisfy this demand for the present flames. The sen-  
 36 sitive appropriate ranges for each case were assessed

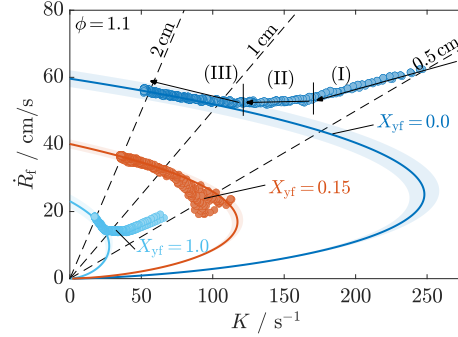


Fig. 2: Propagation speed-stretch rate dependence at 3 bar, 333 K,  $\phi = 1.1$  with increasing R1234yf mole fraction  $X_{yf}$ . Symbols: experiments; lines: nonlinear extrapolations; color bands:  $1\sigma$  confidence intervals for extrapolation data range variation; (I) ignition kernel propagation, (II) transition, and (III) normal flame propagation regime.

according to the procedures described by Hesse et al. [8] using the Markstein lengths from the optical data. For cross-validation, the extrapolated results to  $p_0$  and  $T_0$  from the pressure-rise evaluation (denoted with 'p') and  $S_{L,u}^0$  from the optical evaluation (denoted with 'o') can be compared, as shown in Fig. 3. The upper limit for pressure data extrapolation is associated with the inflection point of the pressure-time history to exclude flame wall interactions. Equivalent visualizations to Figs. 2 and 3 for the other measurement conditions are provided in the Supplementary materials.

To establish a connection between standard conditions that are typically used for fire-safety assessment of refrigerants, but are less precise to measure di-

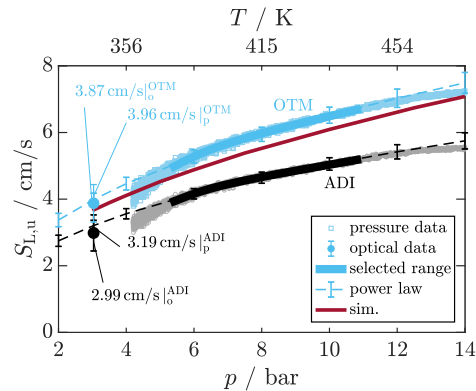


Fig. 3:  $S_{L,u}$  of R1234yf/air ( $\phi = 1.1$ ) at  $p_0 = 3 \text{ bar}$ ,  $T_0 = 333 \text{ K}$ , with and without radiation correction represented by blue and black points, respectively. Power law extrapolation to  $p_0$  and  $T_0$  (dashed lines) with error bars; Optical method results (filled points); Simulations (solid red line).

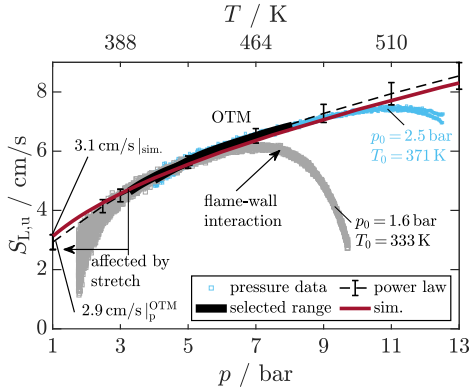


Fig. 4:  $S_{L,u}^0$  of R1234yf/air ( $\phi = 1.3$ ) along near-isentropic compression lines corresponding to 1 atm and 298 K, with radiation correction; Initial condition:  $p_0 = 1.6$  bar,  $T_0 = 333$  K (black), and  $p_0 = 2.5$  bar,  $T_0 = 371$  K (light blue).

1 rectly due to stretch effects, we conducted tests along  
 2 the corresponding pressure and temperature isentrope  
 3 for R1234yf/air mixtures with an equivalence ratio of  
 4 1.3. The results are shown in Fig. 4 for  $p_0 = 1.6$  bar,  
 5  $T_0 = 333$  K and  $p_0 = 2.5$  bar,  $T_0 = 371$  K. Data of multiple  
 6 measurements overlap in the 3 bar to 5 bar range.  
 7 For  $p$  and  $T$  below this range, data are affected by  
 8 stretch since the flames are still too small and do not  
 9 resemble a near-planar flame, which becomes appar-  
 10 ent from the downward bend of the data points. After  
 11 this range, measurements corresponding to ignitions  
 12 at  $p_0 = 1.6$  bar are affected by flame wall interactions,  
 13 whereas measurements conducted at  $p_0 = 2.5$  bar  
 14 provide reliable data up to 8 bar. Combining both sets  
 15 and extrapolating them to standard conditions yields  
 16  $S_{L,u}^0 = 2.9$  cm/s. In comparison, Takizawa et al. [4]  
 17 obtained 1.4 cm/s under  $\mu g$  without considering radi-  
 18 ation and potentially large stretch effects.

19 Unstretched  $S_{L,u}^0$  of the neat refrigerant/air mix-  
 20 tures as a function of the fuel-air equivalence ratio  
 21 are shown in Fig. 5 for the two limiting cases of adi-  
 22 baticity (ADI) and optically thin model (OTM) ra-  
 23 diation. Estimated radiation effects are in the order  
 24 of 14 % for peak R32/air flames to 40 % for rich  
 25 R1234yf/air flames, with ADI being the reference  
 26 condition. Data for R32 of the present study using  
 27 the pressure-rise method are also compared to previ-  
 28 ous results by Hesse et al. [12] using radiation-corrected  
 29 optical measurements. Measurement results are con-  
 30 sistent up to an equivalence ratio of 1.4, where the  
 31 new data are about 0.3 cm/s (6 %) slower, which is  
 32 within the experimental uncertainties.

33 Figure 6 represents the two refrigerants' blending  
 34 behavior regarding their  $S_{L,u}^0$  at  $\phi = 1.1$ . We observe  
 35 a strong nonlinear behavior with increasing  $X_{yf}$ . For  
 36 mixtures  $X_{yf} \geq 0.5$ ,  $S_{L,u}^0$  changes only within experi-  
 37 mental uncertainty limits. A similar trend was re-  
 38 ported by Takizawa et al. [7] as shown in the figure  
 39 for peak velocities at standard conditions without ra-

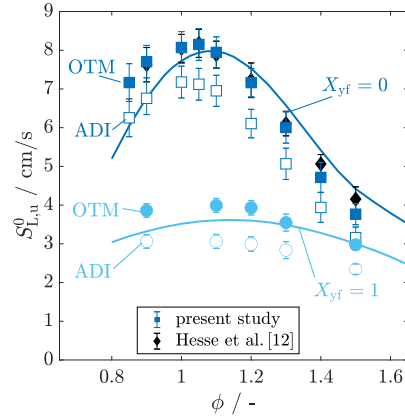


Fig. 5:  $S_{L,u}^0$  of R32/air (dark blue) and R1234yf/air (light blue) over  $\phi$  from the pressure-rise method at  $p_0 = 3$  bar,  $T_0 = 333$  K, without and with radiation corrections (ADI and OTM). Symbols and lines show measured and computed results, respectively.

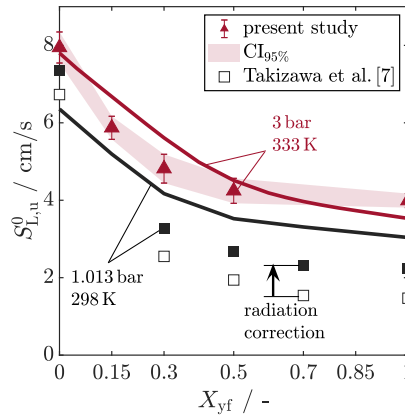


Fig. 6:  $S_{L,u}^0$  blending effect of R32/air with R1234yf ( $X_{yf}$ ) at  $\phi = 1.1$ ,  $p_0 = 3$  bar,  $T_0 = 333$  K (red). Reference from Takizawa et al. [7] for blend peak velocities at  $p_0 = 1.013$  bar,  $T_0 = 298$  K (black), with and without radiation correction. Symbols and lines show measured and computed results, respectively.

40 diation corrections. For comparison, Takizawa et al.'s  
 41 results are also shown with radiation-heat loss esti-  
 42 mated from the present study.

#### 4.3. Predictions with the kinetic model

44 Flame speed simulations of adiabatic, planar sta-  
 45 tionary flames were performed using the open-source  
 46 code FlameMaster [20]. Predicted  $S_{L,u}^0$  results shown  
 47 in Figs. 3 to 6 were obtained with the detailed model  
 48 of Babusok et al. [21], which contains 113 species and  
 49 1064 reactions describing the combustion process of  
 50 R32 and R1234yf.

51 Figure 5 compares radiation-corrected measure-  
 52 ments (OTM) to simulation results for several fuel-

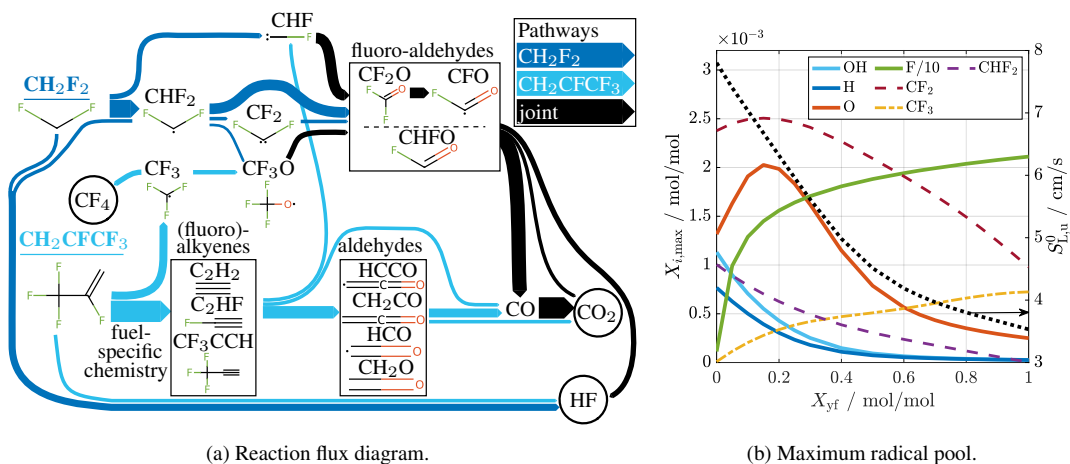


Fig. 7: (a) Schematic reaction flux diagram for HF, CO<sub>2</sub>, CF<sub>2</sub>O, and CF<sub>4</sub> production. Dark blue pathways are attributed to R32 (CH<sub>2</sub>F<sub>2</sub>), light blue pathways to R1234yf (CH<sub>2</sub>=CFCF<sub>3</sub>), and black pathways to their joint chemistry in blends; (b) Maximum molar radical fraction (left *y*-axis) and  $S_{L,u}^0$  (right *y*-axis) as function of  $X_{yf}$  for  $\phi = 1.1$ , 3 bar, and 333 K. Peak radical molar fractions are reached in the reaction zone, except for F (scaled by 1/10), which increases toward burned equilibrium.

1 air equivalence ratios. For reference, measurements  
 2 without radiation correction (ADI) representing a  
 3 lower bound are included. The comparison illustrates  
 4 the importance of accounting for radiation effects  
 5 when validating kinetic model predictions against  
 6 slow flame propagation data. Neglect of radiation  
 7 may even lead to faulty conclusions about a model's  
 8 prediction accuracy, as is clear from the experimental  
 9 results obtained for lean mixtures. The shape of the  
 10 experimental and predicted results is well-matched  
 11 for R32/air flame speeds. However, compared to the  
 12 experiments, the predicted peak is shifted so that  
 13  $S_{L,u}^0$  is underpredicted on the lean side while slightly  
 14 overpredicted for rich conditions. Deviations observed  
 15 for mixtures leaner than  $\phi = 1.0$  exceed the estimated  
 16 experimental uncertainties and are attributed to kinetic  
 17 model uncertainty. Flame speeds of R1234yf/air mixtures  
 18 are underpredicted by the kinetic model for mixture  
 19 leaner than  $\phi = 1.3$ .

20 Predictions for R1234yf/air mixtures along the  
 21 isentropic compression lines in Figs. 3 and 4 are  
 22 compared to radiation-corrected experiments (OTM).  
 23 In the first case, at  $p_0 = 3$  bar,  $T_0 = 333$  K and  
 24  $\phi = 1.1$ , kinetic model predictions deviate from the  
 25 experimental results' lower uncertainty range by 4%.  
 26 The pressure and temperature dependence of  
 27  $S_{L,u}^0$  is matched by the simulations, as evident from  
 28 the similar slope and curvature. Predictions for the  
 29 richer second case along the isentropic compression  
 30 line corresponding to standard conditions (cf. Fig. 4)  
 31 are within experimental uncertainties for pressures  
 32 and temperatures simultaneously increasing up to 12  
 33 bar and 520 K.

34 Lastly, the blending behavior of R1234yf in R32 is  
 35 investigated numerically. Simulations show a similar  
 36 nonlinear flame speed inhibition as experiments  
 37 that levels off for  $X_{yf} > 0.5$ . For marginal R1234yf-  
 38 addition, experiments indicate a more distinct flame  
 39 speed inhibition than model predictions. The over-

40 all trend continues for standard conditions, which is  
 41 in agreement with Takizawa et al.'s data [7]. Despite  
 42 the retrospective radiation correction, Takizawa's  
 43 absolute  $S_{L,u}$  is not matched by the chemical kinetic  
 44 model, which may originate from non-negligible  
 45 stretch influence, as discussed in the previous section.

#### 4.4. Reaction flux and sensitivity analysis

46 The qualitative flux diagram describing  
 47 the consumption of R32 (CH<sub>2</sub>F<sub>2</sub>) and  
 48 R1234yf (CH<sub>2</sub>=CFCF<sub>3</sub>) to form the products HF,  
 49 CO<sub>2</sub>, CF<sub>2</sub>O, and CF<sub>4</sub> is shown in Fig. 7a. The  
 50 principal pathway for R32 involves the formation  
 51 of the difluoromethyl radical CHF<sub>2</sub>, which  
 52 undergoes subsequent reactions with O and O<sub>2</sub> to  
 53 yield fluoro-aldehydes. These aldehydes then  
 54 decompose, producing HF and CO. In many  
 55 aspects, difluoromethane pathways resemble  
 56 methane oxidation, with fluorine replacing  
 57 hydrogen atoms. In contrast, the fuel-specific  
 58 chemistry of R1234yf forms (fluoro)-alkynes  
 59 whose oxidation to aldehydes and subsequently  
 60 CO relies on atomic oxygen due to the higher  
 61 stability of the triple bonds. For both fuels,  
 62 CO<sub>2</sub> is predominantly produced from oxidizing  
 63 CO.

64 The fuel-specific systems of R32 and R1234yf  
 65 are well-separated, except for two minor  
 66 interactions. First, R1234yf consumption  
 67 produces CF<sub>3</sub> radicals, which are subsequently  
 68 oxidized to CF<sub>2</sub>O. Second, R1234yf produces  
 69 C<sub>2</sub>HF, which reacts with atomic oxygen to  
 70 form CHF diradicals. CF<sub>4</sub> acts as a fluorine  
 71 sink, which becomes increasingly important for  
 72 large F/H-ratio refrigerants, such as R1234yf.  
 73 In contrast to the formation of CO<sub>2</sub>, HF is  
 74 more directly produced by the fuel-specific  
 75 chemistry and partly by the reactions of  
 76 fluoro-aldehydes.

Figure 7b presents how the radical pool and  
 $S_{L,u}^0$  change with  $X_{yf}$ . Peak radical molar  
 fractions of H,

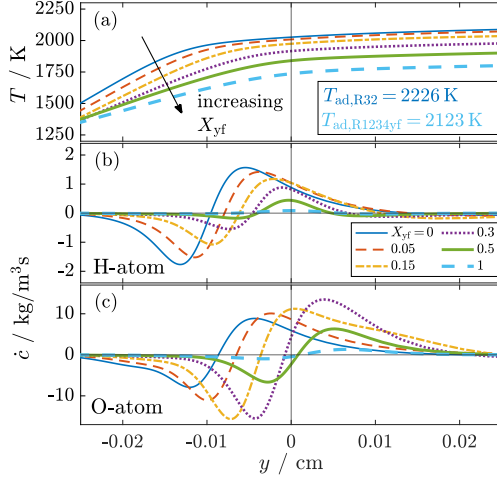


Fig. 8: (a) Temperature; (b) H production rate; (c) O production rate as a function of the flame coordinate  $y$  with the origin at OH peak concentration. Conditions are  $p_0 = 3$  bar,  $T_0 = 333$  K, and  $\phi = 1.1$ .

1 OH, and  $\text{CHF}_2$  decrease with a similar trend as  $S_{L,u}^0$ ,  
 2 whereas O first increases and then follows the trend of  
 3  $S_{L,u}^0$ . R1234yf-addition lowers the H-atom mole fraction  
 4 via HF formation, effectively trapping the radicals and  
 5 shutting down the chain branching, as explained below.  
 6 Thus, fuel consumption must switch to the F-species  
 7 radical-driven reactions, which are slower. The lack of  
 8 available H-atoms also terminates conversions of F so  
 9 that it remains an equilibrium product, as apparent from  
 10 the strong rise in the post-reaction zone.

12 As in hydrocarbon combustion, the laminar flame  
 13 speed of fluorinated compounds is closely related to  
 14 the flame temperature in the main reaction layer. The  
 15  $T$ -profiles for varying  $X_{yf}$  are depicted in Fig. 8a.  
 16 The length of the post-flame zone increases with  $X_{yf}$ .  
 17 Differences in adiabatic flame temperatures between  
 18 neat R32 and R1234yf are 103 K. However, the temper-  
 19 atures in the reaction layer vary significantly more  
 20 by approximately 290 K (at  $y = 0$ ). In Fig. 8b, the  
 21 net production rates  $\dot{c}$  of H highlight not only the  
 22 reduced amount of H radicals but also their withdrawal  
 23 from the fuel-consumption region. Net production and  
 24 consumption of O radicals, shown in Fig. 8c, are  
 25 also displaced toward larger flame coordinates. How-  
 26 ever, increasing  $X_{yf}$  first boosts O radicals before they  
 27 decrease in mixtures with  $X_{yf} > 0.3$ .

28 Figure 9 shows normalized sensitivity coefficients  
 29 [22] for the laminar flame speeds of several fuel  
 30 blends. All flame speeds are sensitive to the chain  
 31 branching reaction 38f, which requires H-atoms to  
 32 take place. Accordingly, the H-atom-producing  
 33 reactions 99f and 294f increase  $S_{L,u}^0$  while H-atom-  
 34 consuming reactions, such as 284f and 363f, decrease  
 35 it. In particular, the sensitivity coefficients of  
 36 reactions 284f and 294f illustrate that the availabil-  
 37 ity of H-atoms from fuel-specific intermediates impacts

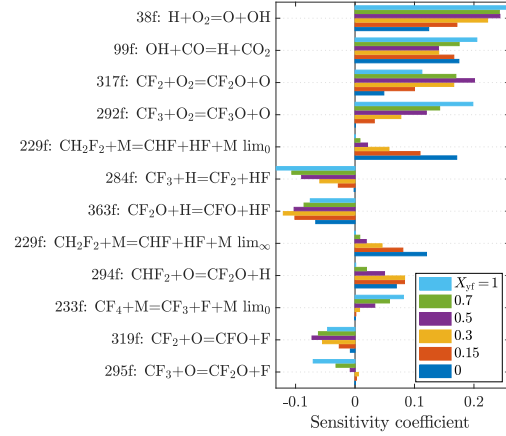


Fig. 9: Normalized sensitivity coefficients for  $S_{L,u}^0$  with respect to frequency factors of rate coefficients at 3 bar, 333 K,  $\phi = 1.1$ , and varying  $X_{yf}$ .

38  $S_{L,u}^0$  ( $\text{CF}_3$  for R1234yf,  $\text{CHF}_2$  for R32). In addition,  
 39 the sensitivity analyses reveal that unimolecular de-  
 40 composition reactions (229f and 233f) and reactions  
 41 with  $\text{O}_2$  and O (317f, 292f, 319f, 295f), which con-  
 42 vert  $\text{CF}_3$  and  $\text{CF}_2$  to the product  $\text{CF}_2\text{O}$ , significantly  
 43 affect  $S_{L,u}^0$ .

## 44 5. Concluding Remarks

45 In the present study, we explored the nonlinear  
 46 blending effect on the laminar flame speed of  
 47 R1234yf and R32 mixtures by conducting high-  
 48 fidelity experiments using the optical and pressure-  
 49 rise methods under microgravity and terrestrial grav-  
 50 ity and correcting results for radiation heat losses. To  
 51 minimize contamination of  $S_{L,u}^0$  values by stretch  
 52 effects, we increased the initial conditions to pres-  
 53 sure and temperature of 3 bar and 333 K. However,  
 54 we also provided data for R1234yf that allows for  
 55 robust extrapolation to standard conditions for com-  
 56 parison with literature data. This study underscores  
 57 the necessity of implementing the aforementioned  
 58 measures for slowly propagating flames to achieve  
 59 experimental data accuracy suitable for refining  
 60 kinetic models via comparisons to adiabatic, planar  
 61 stationary flame simulations. Despite the promising  
 62 predictions of the selected kinetic model for our  
 63 measurements involving neat R32 and R1234yf,  
 64 it was unable to completely account for the sub-  
 65 stantial nonlinear decrease in flame speed observed  
 66 in the experiments. We analyzed the chemical  
 67 kinetic model using flux and sensitivity analyses  
 68 to understand the chemical interactions involved  
 69 in blending these refrigerants. With R1234yf-  
 70 addition, H-atoms react to form HF, trapping them  
 71 and shutting down the typical hydrocarbon chain-  
 72 branching reactions. Our sensitivity analysis  
 73 highlights key reactions involving fuel-specific  
 74 intermediates:  $\text{CHF}_2$  for R32, providing H-atoms,  
 and  $\text{CF}_3$  for R1234yf, removing H-atoms. Thus, R1234yf-

1 addition has an attenuating effect on the flame tem- 58  
2 perature and produces an extended post-flame zone, 59  
3 which yields a strong decrease in  $S_{L,u}^0$ . 60

#### 4 Declaration of competing interest 61

5 The authors declare that they have no known com- 64  
6 peting financial interests or personal relationships that 65  
7 could have appeared to influence the work reported in 66  
8 this paper. 67

#### 9 Acknowledgments 68

10 The authors from RWTH gratefully acknowl- 72  
11 edge the financial support partly provided by the 73  
12 Deutsches Zentrum für Luft und Raumfahrt (DLR, 74  
13 German Aerospace Center), Grant no. 50WM2258. 75  
14 Co-authors from NIST obtained financial support 76  
15 under contract DE-EE0007615 from the Office of 77  
16 Energy Efficiency and Renewable Energy, U.S. 78  
17 Department of Energy, and the U.S. Department 79  
18 of Defense, Strategic Environmental Research and 80  
19 Development Program (SERDP), under contract 81  
20 W74RDV91831838. We thank the European Space 82  
21 Agency (ESA) for funding and the Center of Ap- 83  
22 plied Space Technology and Microgravity (ZARM) 84  
23 for contracting the drops in the GTB Pro. 85

#### 24 Supplementary material 86

25 Supplementary material associated with this article 87  
26 can be found in the online version. 88

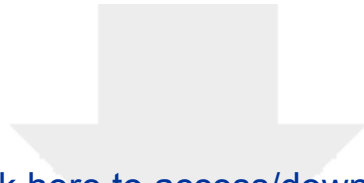
#### 27 References 89

28 [1] Ø. Hodnebrog, B. Aamaas, J. S. Fuglestedt, 95  
29 G. Marston, G. Myhre, C. J. Nielsen, M. Sandstad, 96  
30 K. P. Shine, T. J. Wallington, Updated global warm- 97  
31 ing potentials and radiative efficiencies of halocarbons 98  
32 and other weak atmospheric absorbers, *Rev. Geophys.* 99  
33 58 (3) (2020). 100  
34 [2] K. Thu, K. Takezato, N. Takata, T. Miyazaki, Y. Hi- 101  
35 gashi, Drop-in experiments and exergy assessment of 102  
36 HFC-32/HFO-1234yf/R744 mixture with GWP below 103  
37 150 for domestic heat pumps, *Int. J. Refrig* 121 (2021) 104  
38 289–301. 105  
39 [3] K. Takizawa, A. Takahashi, K. Tokuhashi, S. Kondo, 106  
40 A. Sekiya, Burning velocity measurement of fluo- 107  
41 rinated compounds by the spherical-vessel method, 108  
42 *Combust. Flame* 141 (3) (2005) 298 – 307. 109  
43 [4] K. Takizawa, K. Tokuhashi, S. Kondo, Flammabil- 110  
44 ity assessment of  $\text{CH}_2\text{CFCF}_3$ : Comparison with fluo- 111  
45 roalkenes and fluoroalkanes, *J. Hazard. Mater.* 172 (2) 112  
46 (2009) 1329 – 1338. 113  
47 [5] D. Clodic, T. Jabbour, Method of test for burning ve- 114  
48 locity measurement of flammable gases and results, 115  
49 *HVAC&R Research* 17 (1) (2011) 51–75. 116  
50 [6] P. Papas, S. Zhang, W. Kim, S. Zepieri, M. Colket, 117  
51 P. Verma, Laminar flame speeds of 2,3,3,3- 118  
52 tetrafluoropropene mixtures, *Proc. Combust. Inst.* 36 (1) (2016) 1145–1154. 119  
53 [7] K. Takizawa, Flammability assessment of 120  
54  $\text{CH}_2=\text{CFCF}_3$  (R-1234yf) and its mixtures with 121  
55  $\text{CH}_2\text{F}_2$  (R-32), in: *Int. Symp. Next-gen. Air-Con.* 122  
56 *Refrig. Technol.*, 2010. 123

[8] R. Hesse, C. Bariki, M. J. Hegetschweiler, G. T. Lin- 58  
teris, H. Pitsch, J. Beeckmann, Elucidating the chal- 59  
lenges in extracting ultra-slow flame speeds in a closed 60  
vessel—A  $\text{CH}_2\text{F}_2$  microgravity case study using op- 61  
tical and pressure-rise data, *Proc. Combust. Inst.* 39 62  
(2022). 63  
[9] C. Needham, P. Westmoreland, Combustion and 64  
flammability chemistry for the refrigerant hfo- 65  
1234yf (2,3,3,3-tetrafluoropropene), *Combust. Flame* 184 (Supplement C) (2017) 176 – 185. 66  
[10] V. Babushok, D. Burgess, D. Kim, M. Hegetschweiler, 67  
G. Linteris, Modeling of combustion of fluorine- 68  
containing refrigerants, NIST Technical Note 2170 69  
(2021). 70  
[11] A. Kelley, J. Bechtold, C. Law, Premixed flame propa- 71  
gation in a confining vessel with weak pressure rise, *J.* 72  
*Fluid Mech.* 691 (2012) 26–51. 73  
[12] R. Hesse, L. Berger, C. Bariki, M. J. Hegetschweiler, 74  
G. T. Linteris, H. Pitsch, J. Beeckmann, Low global- 75  
warming-potential refrigerant  $\text{CH}_2\text{F}_2$  (R-32): Integra- 76  
tion of a radiation heat loss correction method to ac- 77  
curately determine experimental flame speed metrics, 78  
*Proc. Combust. Inst.* 38 (3) (2020) 4665–4672. 79  
[13] J. K. Tavares, V. Gururajan, J. Jayachandran, Ef- 80  
fects of radiation heat loss on planar and spheri- 81  
cal hydrofluorocarbon/air flames, *Combust Flame* 258 82  
(2023) 113067. 83  
[14] J. Santner, F. Haas, Y. Ju, F. Dryer, Uncertainties in 84  
interpretation of high pressure spherical flame propa- 85  
gation rates due to thermal radiation, *Combust. Flame* 161 (1) (2014) 147–153. 86  
[15] C. Bariki, R. Hesse, F. Halter, H. Pitsch, J. Beeckmann, 87  
Combined isochoric and isobaric acquisition method- 88  
ology for accurate flame speed measurements from 89  
ambient to high pressures and temperatures, *Proc.* 90  
*Combust. Inst.* 38 (2) (2020) 2185–2193. 91  
[16] M. Elia, M. Ulinski, M. Metghalchi, Laminar Burning 92  
Velocity of Methane–Air–Diluent Mixtures, *J. Eng.* 93  
*Gas Turbines Power* 123 (1) (2000) 190–196. 94  
[17] M. Hegetschweiler, G. T. Linteris, Data reduction 95  
tool for spherical constant volume flame experiments, 96  
NIST Technical Note 2148 (2021). 97  
[18] K. Takizawa, A. Takahashi, K. Tokuhashi, S. Kondo, 98  
A. Sekiya, Reaction stoichiometry for combustion of 99  
fluoroethane blends, *ASHRAE Transactions* 112 (2) 100  
(2006) 459–469. 101  
[19] J. Beeckmann, R. Hesse, J. Schaback, H. Pitsch, 102  
E. Varea, N. Chaumeix, Flame propagation speed and 103  
markstein length of spherically expanding flames - 104  
assessment of extrapolation and measurement tech- 105  
niques, *Proc. Combust. Inst.* 37 (2019) 1521–1528. 106  
[20] H. Pitsch, R. Langer, Flamemaster: A C++ computer 107  
program for 0D combustion and 1D laminar flame cal- 108  
culations, version 4.4.0 (2023). 109  
[21] V. Babushok, D. Burgess Jr, M. Hegetschweiler, 110  
G. Linteris, Flame propagation in the mixtures of 111  
 $\text{O}_2/\text{N}_2$  oxidizer with fluorinated propene refrigerants 112  
( $\text{CH}_2\text{CFCF}_3$ ,  $\text{CHFCHCF}_3$ ,  $\text{CH}_2\text{CHCF}_3$ ), *Combust.* 113  
*Sci. Technol.* (2020) 1–24 114  
[22] R. Langer, J. Lotz, L. Cai, F. vom Lehn, K. Leppkes, 115  
U. Naumann, H. Pitsch, Adjoint sensitivity analysis of 116  
kinetic, thermochemical, and transport data of nitro- 117  
gen and ammonia chemistry, *Proc. Combust. Inst.* 38 118  
(2021) 777–785. 119  
120  
121



Click here to access/download  
**Supplemental Material**  
species\_dict.pdf



Click here to access/download

**Supplemental Material**

CI\_2024\_supplementary\_material.pdf

